


Distinct functional developments of surviving and eliminated presynaptic terminals

Mitsuharu Midorikawa^{a,1} and Mariko Miyata^{a,1} 

^aDivision of Neurophysiology, Department of Physiology, School of Medicine, Tokyo Women's Medical University, Tokyo 162-8666, Japan

Edited by Thomas C. Südhof, Stanford University, Stanford, CA, and approved February 8, 2021 (received for review October 27, 2020)

For neuronal circuits in the brain to mature, necessary synapses must be maintained and redundant synapses eliminated through experience-dependent mechanisms. However, the functional differentiation of these synapse types during the refinement process remains elusive. Here, we addressed this issue by distinct labeling and direct recordings of presynaptic terminals fated for survival and for elimination in the somatosensory thalamus. At surviving terminals, the number of total releasable vesicles was first enlarged, and then calcium channels and fast-releasing synaptic vesicles were tightly coupled in an experience-dependent manner. By contrast, transmitter release mechanisms did not mature at terminals fated for elimination, irrespective of sensory experience. Nonetheless, terminals fated for survival and for elimination both exhibited developmental shortening of action potential waveforms that was experience independent. Thus, we dissected experience-dependent and -independent developmental maturation processes of surviving and eliminated presynaptic terminals during neuronal circuit refinement.

synapse | presynapse | presynaptic development

The developmental maturation of neural circuits involves the initial formation of a surplus of synapses, followed by selective survival of strengthened synapses and elimination of others. This selective pruning occurs throughout the brain and is considered a fundamental event for the maturation of neuronal networks. Extensive studies have been performed to understand the underlying mechanisms (1, 2), and several model systems in the developing brain have been proposed (3–6). Such studies have shown that this refinement process is remarkably sensitive to sensory experience during postnatal development (5, 7), indicating that the strengthening of winner synapses and elimination of loser synapses occurs in an experience-dependent manner. However, it is not known if the transmitter release mechanism, crucial for synaptic transmission, develops differently at presynaptic terminals that are fated for survival and at those fated for elimination. Furthermore, how sensory experience affects presynaptic functional development is not clear because direct observations are lacking.

To examine transmitter release kinetics, the most direct methods are capacitance measurements of presynaptic terminals or paired recordings from a presynaptic terminal and postsynaptic cell (8, 9). However, these require patch clamping directly on presynaptic terminals, which is often not possible because of their small size at most central nervous system synapses. These methods have been applied to large presynaptic structures (10–13), but presynaptic functional changes before circuit maturation have only been explored at the calyx of Held presynaptic terminal (14–20), and the transmitter release properties from terminals fated for elimination remain mostly unknown.

To address these issues, we focused on the rodent whisker sensory pathway, in which sensory fiber synapses onto excitatory thalamocortical neurons of the somatosensory thalamus have been used to study experience-dependent circuit development. In rodents, whisker-mediated sensory information is transmitted via glutamatergic afferents (lemniscal fibers) from the V2 region of the principal trigeminal nucleus (PrV2) to the somatosensory

thalamus (the ventral posteromedial nucleus [VPM]). It has been shown that VPM neurons also receive ectopic innervation from fibers originating from non-PrV2 regions, but these synapses are eliminated during circuit maturation (7). The elimination of these ectopic connections is prevented by whisker deprivation (WD), indicating that circuit refinement in the VPM is experience dependent (7). Therefore, transmitter release mechanisms of terminals fated for survival or elimination during development can be examined independently by recording from PrV2-originating lemniscal fiber terminals (whisker-LFTs) or non-PrV2-origin lemniscal fiber terminals (ectopic-LFTs), respectively. Furthermore, experience-dependent modulations of transmitter release mechanisms can be easily examined by employing WD (7).

Here, we used genetic and viral approaches to fluorescently label whisker- and ectopic-LFTs. The labeling enabled us to perform direct patch-clamp recordings from small LFTs and measure capacitance. By also using paired recordings from an LFT and a target VPM neuron, we were able to extensively examine the kinetics of transmitter release at terminals fated for survival or for elimination. Our data show that the transmitter release kinetics at whisker-LFTs exhibited developmental and sensory experience-dependent maturation, whereas ectopic-LFTs remained immature and insensitive to sensory experience. Thus, we clarified the distinct functional developments between “surviving” and “to-be-pruned” presynaptic terminals during neural circuit refinement.

Significance

During neuronal circuit development, there is a surplus of synapses that undergo selective strengthening or elimination via experience-dependent mechanisms. However, the functional differentiation of presynaptic terminals during the refinement process remains elusive. To address this issue, we performed direct electrophysiological recordings selectively from presynaptic terminals fated for survival or elimination in the somatosensory thalamus during neural circuit refinement. With development, the transmitter release mechanisms matured in an experience-dependent manner at surviving presynaptic terminals but not at those that were later eliminated. However, the maturation of action potential waveforms was indistinguishable between surviving and eliminated terminals. Thus, we clarified a distinct functional development of presynaptic terminals fated for survival and for elimination during neuronal circuit refinement.

Author contributions: M. Midorikawa and M. Miyata designed research; M. Midorikawa performed research; M. Midorikawa analyzed data; and M. Midorikawa and M. Miyata wrote the paper.

The authors declare no competing interest.

This article is a PNAS Direct Submission.

Published under the PNAS license.

¹To whom correspondence may be addressed. Email: midorikawa.mitsuharu@twmu.ac.jp or mmiyata@twmu.ac.jp.

This article contains supporting information online at <https://www.pnas.org/lookup/suppl/doi:10.1073/pnas.2022423118/-DCSupplemental>.

Published March 9, 2021.

Results

Distinct and Direct Measurements of Transmitter Release Kinetics from Whisker- and Ectopic-LFTs. To distinguish whisker- and ectopic-LFTs, we generated Krox20-Ai34D mice, in which whisker-LFTs were identified with tdTomato-tagged synaptophysin (21, 22). Krox20-Ai34D mice were generated by crossing a Krox20-Cre knockin line and a Cre-dependent synaptophysin-tdTomato reporter line (Ai34D). Krox20, a transcription factor in the developing hindbrain, has a specific expression pattern in rhombomere 3, which corresponds to PrV2 (7). Therefore, by crossing Krox20-Cre and Ai34D lines, whisker-LFTs (i.e., PrV2-originating LFTs) were labeled with tdTomato fluorescence (Fig. 1A). The ectopic-LFTs (i.e., non-PrV2-originating LFTs) were selectively labeled by introducing “Cre-off” adeno-associated virus (AAV; AAV9-Ef1a-DO-ChETA-EYFP) (23) into the Krox20-Ai34D mouse brainstem principal trigeminal nucleus (Pr5), including nonwhisker regions (24) (Fig. 1A). The Cre-off vector expresses the encoded protein (i.e., ChETA-EYFP) unless Cre-mediated recombination reverses the orientation of the transgene (23). Thus, whisker-LFTs were labeled with tdTomato, and ectopic-LFTs were labeled with EYFP (Fig. 1B). The fluorescent labeling enabled us not only to distinguish between whisker- and ectopic-LFTs but also to perform direct presynaptic patch-clamp recordings (Fig. 1C). In a 200- to 300- μm parasagittal thalamic acute slice, labeled LFTs were clearly fluorescent and visible for direct patch-clamp recordings (Fig. 1C).

Kinetics of transmitter release were examined by capacitance measurement (25) or by deconvolution of the excitatory postsynaptic current (EPSC) response (26, 27). In a capacitance measurement configuration, depolarizations of presynaptic LFTs induced clear calcium currents and capacitance jumps (Fig. 1D). The amplitudes of capacitance jumps reflect the total increase of membrane surface caused by depolarization-induced exocytosis of synaptic vesicles. Accordingly, the capacitance jumps were blocked by 500 nM tetanus toxin infusion, which blocks synaptic vesicle fusion (*SI Appendix, Fig. S1A and B*). Because membrane capacitance cannot be measured during depolarization, we assessed the time course of exocytosis from postsynaptic EPSCs in addition to examine the time course of exocytosis directly. Under the paired-recording configuration, VPM neuron EPSCs were induced by presynaptic LFT depolarizations (Fig. 1E and F). From the recorded EPSCs, the time course of exocytosis was calculated by deconvolution with asynchronous miniature EPSCs (mEPSCs; postsynaptic responses to single synaptic vesicle release events, *SI Appendix, Fig. S2A–D*), which provided the vesicle release rate. This method was based on the assumption that EPSCs are a linear summation of mEPSCs (27). Because the frequency of the asynchronous mEPSCs was nearly 10-fold higher than that before the stimulus (mean \pm SEM: 3.2 ± 1.1 Hz vs. 31.4 ± 5 Hz, $P < 0.01$, see *SI Appendix, Figs. S2A and S3A* for example traces), we surmised that the asynchronous mEPSCs mostly originated from the recorded LFTs. Integrating this release rate provides the cumulative number of vesicles released at a given time after the stimulus (Fig. 1F) (26, 27). The capacitance jumps and the number of released vesicles calculated from EPSC deconvolutions scaled linearly for depolarizations of 2 to 100 ms (Fig. 1G and H and *SI Appendix, Fig. S3A and B*).

By comparing the capacitance jumps and EPSC deconvolutions, we calculated the connection ratio between single LFTs and target VPM neurons. Whereas capacitance measurements sample the total release from the entire terminal, EPSC deconvolution samples only a fraction of total release from the terminal that is directed toward the single recorded VPM neuron. Therefore, quantitative comparison of the number of released vesicles with both techniques results in an estimate of the number of postsynaptic VPM neurons per LFT for each recording pair. Assuming a single vesicle capacitance of 0.1 fF

(which may vary from 0.07 to 0.1 fF depending on vesicle diameter) (11, 28, 29), the comparison revealed an average of 1.13 VPM neurons per LFT, indicating that a single LFT targeted a single VPM neuron in most cases.

These results validated estimations of transmitter release both by capacitance measurements and by EPSC deconvolutions under our experimental conditions. Therefore, the ability to make direct measurements of transmitter release from single LFTs enabled us to examine functional differences between whisker- and ectopic-LFTs.

Developmental and Experience-Dependent Changes of Transmitter Release Kinetics Occur at Whisker-LFTs but Not at Ectopic-LFTs. The lemniscal fibers show unique developmental innervations, and three developmental phases have been identified (Fig. 2A) (7). In rodents, the first week after birth is a “synapse formation” phase, when a VPM neuron is weakly innervated by several lemniscal fibers. The second week is a “functional differentiation” phase, when connections from several fibers are first strengthened in parallel, and then the number of innervated fibers is reduced thereafter. Individual VPM neurons receive intermingled innervations from whisker [Krox20(+)] and ectopic [Krox20(–)] fibers until the end of the second week. The third week is a “mature” phase, when a VPM neuron is strongly innervated by a single whisker [Krox20(+)] fiber, and ectopic [Krox20(–)] fibers are mostly eliminated. With WD (whisker sensory deprivation from postnatal day 12 [P12]–P13 to the recording day after P16), multiple fiber innervations of a single VPM neuron and ectopic fiber terminals remain in the “mature” phase (Fig. 2A) (7, 30). Therefore, the whisker sensory inputs during the functional differentiation phase drive the selective strengthening of whisker [Krox20(+)] fibers and elimination of ectopic [Krox20(–)] fibers.

Pathway-specific developmental and experience-dependent changes of the transmitter release kinetics were examined by capacitance measurements (Fig. 2B and C). To examine the characteristics of the readily releasable pool (RRP) of synaptic vesicles, capacitance jumps were recorded in response to various durations of depolarization. We defined the size of the RRP as the maximum amount of capacitance jump evoked by depolarizations, which is also termed $\text{RRP}_{\text{depol}}$ or total releasable pool (31). The capacitance jumps correlated positively with basal capacitances (e.g., size), but the basal capacitances varied up to approximately sevenfold (0.55 to 4.1 pF; *SI Appendix, Fig. S4A*). This variability compromised statistical comparisons between different experimental conditions. Therefore, we normalized the capacitance jumps to the basal capacitances. At whisker-LFTs, capacitance jumps at P4–6 were very small, with maximum capacitance jumps (reflecting the total RRP size) estimated to be ~ 4 fF/pF (Fig. 2B, D, and E). This is consistent with previous studies demonstrating that VPM neuron EPSCs induced by lemniscal fiber stimulations were weak before P6 (4, 7). The total RRP sizes at whisker-LFTs enlarged thereafter and, at P8–14, were already comparable to those of mature P16–25 terminals (Fig. 2B, D, and E). The total RRP size per 1 pF was ~ 30 fF (Fig. 2D and E). Considering the capacitance jump per single vesicle fusion of 0.1 fF (28), this corresponds to a total RRP size of ~ 300 vesicles per 1 pF. On the other hand, capacitance jumps of P8–14 ectopic-LFTs were very small, similar to P4–6 whisker-LFTs (Fig. 2C, F, and G). The results indicate that the transmitter release machinery did not develop further at ectopic-LFTs.

Between P8–14 (differentiation phase) and P16–25 (mature phase), the transmitter release kinetics of ectopic-LFTs remained essentially the same, but that of whisker-LFTs further matured. The capacitance jumps after shorter (10 ms or less) depolarizations were significantly larger at P16–25 than under other conditions, indicating a development of the fast component of the RRP,

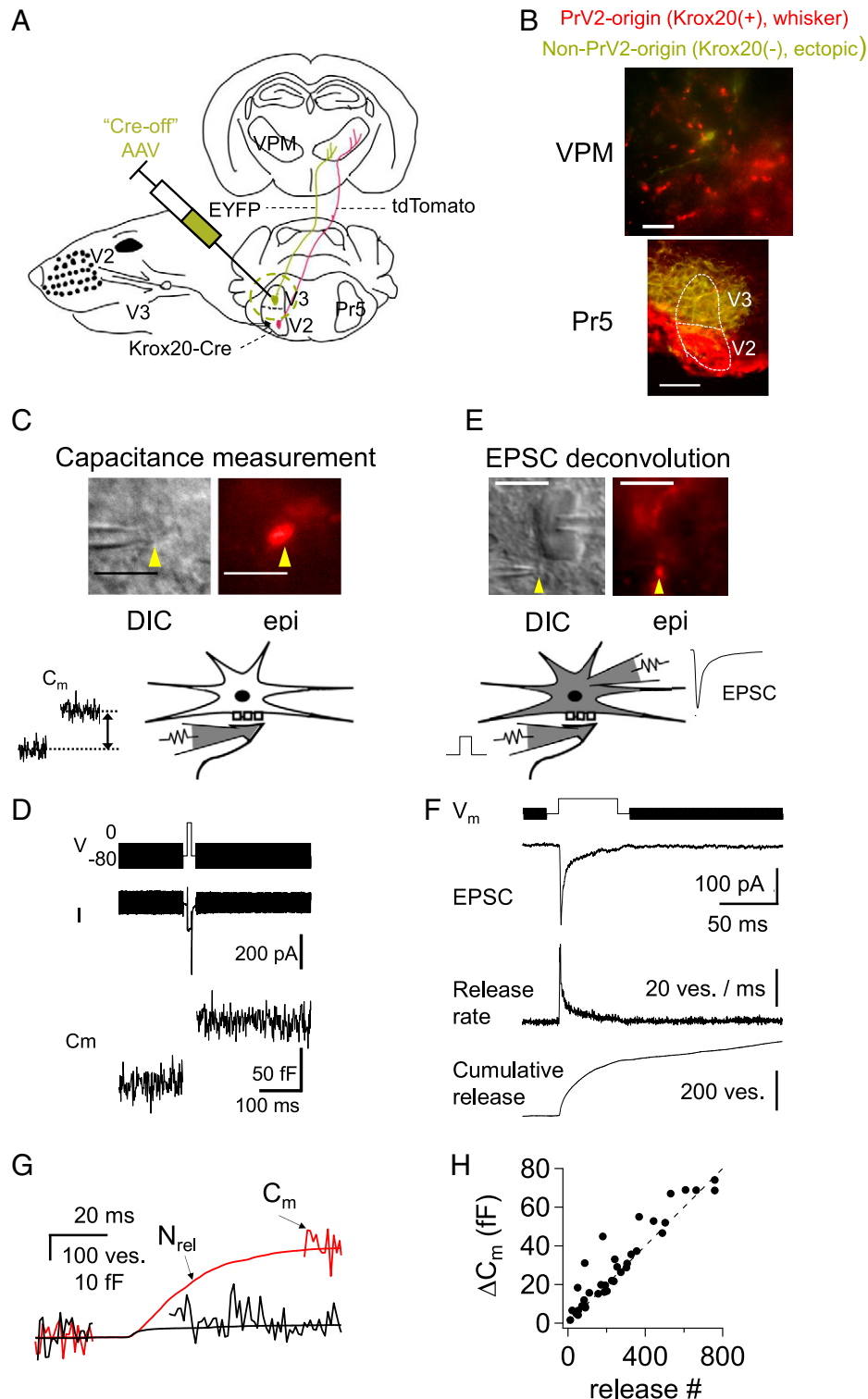


Fig. 1. Direct and selective recordings from whisker- and ectopic-LFTs enabled analysis of pathway-specific transmitter release kinetics. (A) Schematic view of distinct labeling of PrV2-originating [Krox20(+), whisker] and non-PrV2-originating [Krox20(–), ectopic] pathways. (B) Distinct labeling of Krox20-Cre⁺ (i.e., PrV2 origin, whisker) and Krox20-Cre[–] (i.e., non-PrV2 origin, ectopic) pathways by injecting “Cre-off” AAV to Krox20-Ai34D mice. (Scale bars: Top, 20 μm ; Bottom, 500 μm .) The fluorescence signal for Pr5 in the lower-magnification image was amplified by immunostaining. (C) A LFT imaged with DIC (Left) and epifluorescence (Right). (Scale bar: 10 μm .) Bottom shows a schematic view of capacitance measurement configuration. (D) Example traces of depolarization-induced calcium current and C_m jump. (E) A paired recording imaged with DIC (Left) and epifluorescence (Right). (Scale bar: 10 μm .) Bottom shows a schematic view of paired-recording configuration. (F) Example traces of depolarization-induced EPSC from postsynaptic VPM neuron, deconvolved release rate, and cumulative release. (G) Superimposed preterminal capacitance (C_m) and EPSC deconvolution estimated cumulative release number (N_{rel}) from the same recording: 2 ms (black) and 100 ms (red) depolarization-induced responses. (H) The capacitance jumps against EPSC deconvolution-estimated number of vesicles released. Dotted line indicates a 1:1 relation between LFT and VPM neuron based on single-vesicle capacitance as 0.1 fF. $n = 10$ cells. Data for D–H are from whisker-LFTs.

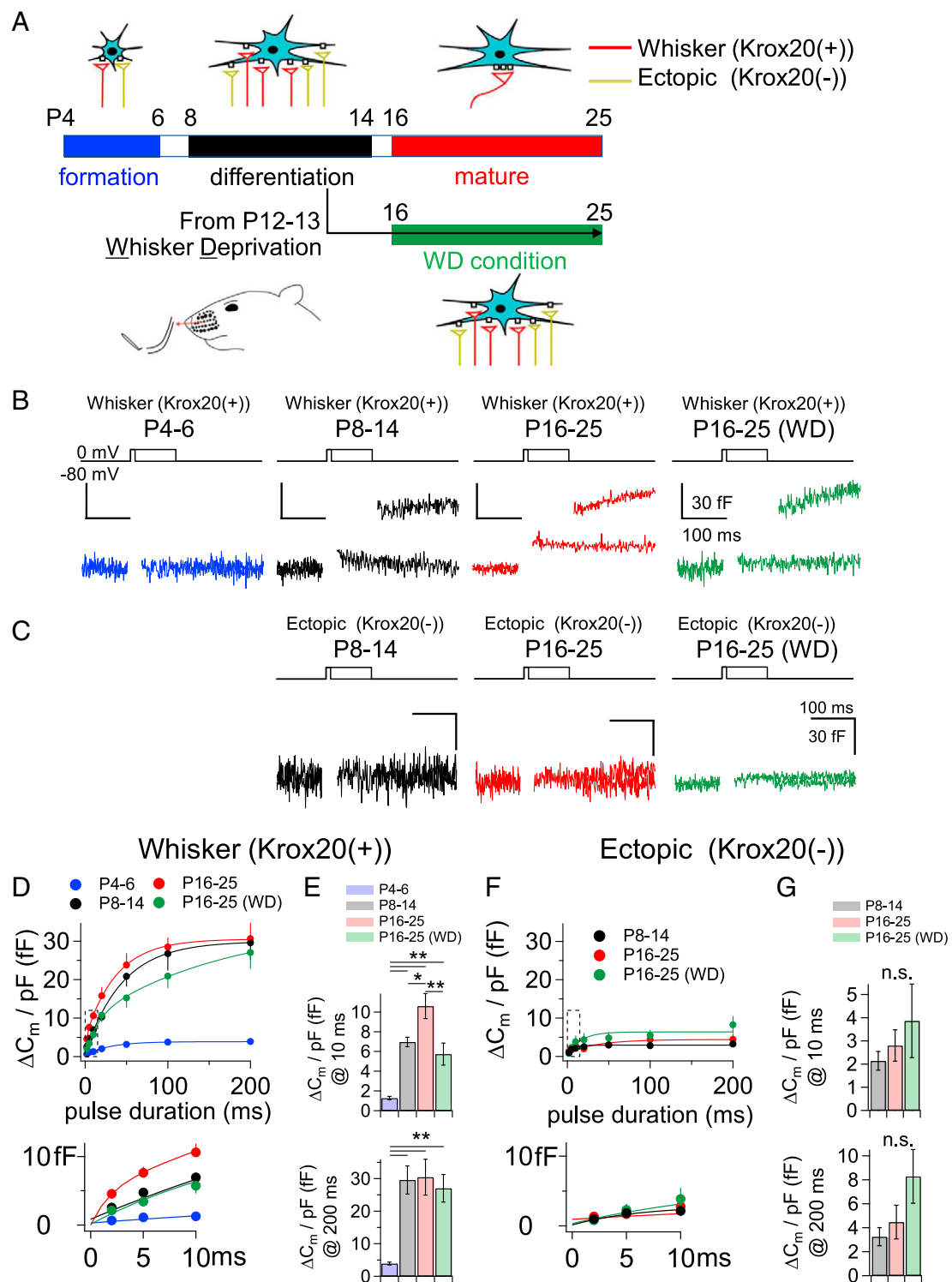


Fig. 2. Readily releasable pool enlarges first, and the fast-releasable pool develops thereafter at whisker-LFTs in an experience-dependent manner, but the readily releasable pool of ectopic-LFTs remains small. (A) Schematic view of experimental conditions. Example of capacitance jumps induced by 10- and 100-ms depolarizations in each condition at whisker-LFTs (B) and at ectopic-LFTs (C). (D) Averaged ΔC_m per picofarad (pF) values were plotted against pulse durations for whisker-LFTs under each condition. Enlarged traces are shown on the *Bottom*. $n = 8$ to 14, 12 to 14, 8 to 18, and 18 to 21, for P4–6, P8–14, P16–25, and WD, respectively. P16–25 responses were significantly larger than those for the three other conditions at pulse durations of 2 ($P < 0.01$), 5 ($P < 0.01$) and 10 ms ($P < 0.05$, one-way ANOVA followed by Tukey's post hoc test). For the pulse durations longer than 20 ms, there were no significant differences between P8–14, P16–25, and P16–25 (WD). P4–6 responses were significantly smaller than those for the three other conditions at all pulse durations ($P < 0.05$, one-way ANOVA followed by Tukey's post hoc test) except for the 2-ms response against WD. (E) Averaged ΔC_m per pF evoked by 10-ms (*Top*) and 200-ms (*Bottom*) depolarizing pulses. (F) Same as in D but for ectopic-LFTs. Enlarged traces are shown on the *Bottom*. $n = 10$ to 11, 5 to 7, and 4 to 5 for P8–14, P16–25, and WD, respectively. There were no significant differences between the three conditions. (G) Same as in E but for ectopic-LFTs. * $P < 0.05$, ** $P < 0.01$, n.s., not significant, one-way ANOVA followed by Tukey's post hoc test. Error bars show SEMs.

which was released with a few-millisecond time constant (Fig. 2 *B, D, and E*) (28). At P16–25 whisker-LFTs, the release time course was fitted by a double exponential, with $\tau = 1.2$ and 54 ms, unlike at P4–6 or at P8–14, when the release time courses were fitted by single exponentials, with $\tau = 28.8$ ms and 44.9 ms, respectively (Fig. 2*D*). On the other hand, the enlargement of the capacitance jumps was not significant when the capacitance jumps were not normalized to the basal capacitances (*SI Appendix, Fig. S4B*). The enlargement of the fast component of transmitter release was verified via paired recordings (see Fig. 4). The development of the fast component of the RRP was accompanied by enhanced vesicle recycling (*SI Appendix, Fig. S5 A and B*). The release time courses of the mature whisker-LFTs were comparable to those of other glutamatergic presynaptic terminals (11, 13, 32).

The developmental changes of the presynaptic transmitter release properties were inconsistent with a previous report showing that the paired-pulse ratios (PPRs) of EPSCs evoked by external single-fiber stimuli did not change from P7 to P24 (4). However, we found that the PPR underwent clear developmental changes (*SI Appendix, Fig. S5 C–E*) by investigating PPRs with various interstimulus intervals under our experimental conditions. When we blocked AMPA [α -amino-3-hydroxy-5-methyl-4-isoxazolepropionic acid] receptor desensitization by applying cyclothiazide and emphasized paired-pulse depletion by raising the external Ca^{2+} concentration from 1.5 mM (4) to 3 mM, we detected a significant difference in PPRs at the different developmental phases (*SI Appendix, Fig. S5 C–E*). The strong effect of desensitization on AMPA EPSC responses and the resultant changes of PPRs, especially at shorter interstimulus intervals, were similar to what has been reported for synapses in the lateral geniculate nucleus synapse (33). Altogether, the results suggest that the RRP for the fast component is developmentally enlarged and accompanied by enhanced vesicle recycling.

Development of the fast component of transmitter release at whisker-LFTs was prevented by WD, indicating that sensory experience is necessary for this process (Fig. 2 *B, D, and E*). On the other hand, capacitance jumps for ectopic-LFTs were not affected by WD (Fig. 2 *C, F, and G*), strongly suggesting that these synapses were not strengthened via inhibition of sensory experience-dependent activity at whisker-LFTs. The results indicate that the enlargement of the fast component of transmitter release at whisker-LFTs is whisker-mediated sensory experience dependent, whereas the development of the transmitter release machinery at ectopic-LFTs is insensitive to sensory experience.

Developmental Changes of Action Potential Waveforms Are Not Pathway Specific. Are the pathway- and experience-dependent modifications specific to the transmitter release kinetics or do they affect other presynaptic properties as well? To answer this question, we examined presynaptic terminal sizes, calcium currents, and action potential (AP) waveforms. We focused on these parameters because they are closely related to transmitter release kinetics. Terminal size correlates with synaptic strength in some synapses (7, 34), and calcium currents and AP waveforms strongly affect transmitter release, as they are directly related to the kinetics of the calcium influx that triggers exocytosis.

Terminal sizes were evaluated by basal membrane capacitance, and calcium currents (assessed as calcium current density) were evoked by applying depolarization to 0 mV. The basal membrane capacitance and calcium current density of whisker-LFTs increased from P4–6 to P8–14 (mean \pm SEM: basal capacitance, from 1.59 ± 1.1 pF to 2.28 ± 1.4 pF; calcium current density, from 10.2 ± 1.2 pA/pF to 23.3 ± 2.4 pA/pF, respectively), but those of ectopic-LFTs showed no developmental changes (Fig. 3 *A–D*). Basal capacitance and calcium current density of ectopic-LFTs were similar to those of P4–6 whisker-LFTs throughout the development phases (Fig. 3 *B and D*). The calcium current amplitudes were consistent with the current

densities (*SI Appendix, Fig. S6 A and B*). These results suggest that at ectopic-LFTs, not only the transmitter release kinetics but also terminal sizes and calcium currents remain immature during development. The results also suggest that the enlargement of the fast component of RRP between P8–14 and P16–25 was not caused by a change of calcium influx kinetics, as current density as well as the rise time of calcium currents remained unchanged (mean \pm SEM: 0.79 ± 0.13 ms and 0.65 ± 0.12 ms at P8–14 and P16–25, respectively, $P = 0.44$).

APs were evoked with 1-ms current injections under current clamp mode. AP waveforms at other synapses become shorter with development (14, 16, 35). LFTs are no exception, as they also exhibited developmental shortening. In contrast to the terminal sizes and calcium currents, the time course of developmental shortening of AP waveforms was not different between whisker- and ectopic-LFTs (Fig. 3 *E–G*). With development, the full width at half maximum (FWHM) of APs gradually became shorter, reaching ~ 0.2 ms at maturation (Fig. 3*G*). On the other hand, peak AP amplitudes increased at P8–14, unlike peak AP amplitudes at the calyx of Held, which remain constant throughout development (14, 15). This suggests a delayed up-regulation of K^+ conductance compared with that of Na^+ conductance. The developmental change in peak AP amplitudes occurred in both whisker- and ectopic-LFTs (*SI Appendix, Fig. S6 C–E*). To our surprise, WD manipulation did not affect the terminal size (Fig. 3*A*), calcium current (Fig. 3*C*), or AP waveform (Fig. 3 *E and G* and *SI Appendix, Fig. S6 C and E*), suggesting that these properties are experience independent during development.

Fast Component of Transmitter Release Is Advantageous for AP-Evoked Transmitter Release.

The results so far indicate that the prominent developmental change of whisker-LFTs between P8–14 and P16–25 is the enhancement of the fast component of transmitter release. To examine this directly and with submillisecond time resolution, we performed EPSC deconvolution analysis against EPSCs evoked by whisker-LFT depolarization under a paired-recording configuration. The calculated release time courses were fitted by double exponentials, which correspond to the fast and slow components of transmitter release, clearly revealing the enhancement of the fast component of transmitter release at whisker-LFTs at P16–25 compared with that at P8–14 (mean fraction \pm SEM: 0.16 ± 0.03 vs. 0.07 ± 0.02 , respectively, $P = 0.02$; Fig. 4 *A and B*). This enhancement was abolished under the WD condition (mean fraction \pm SEM: [P16–25] 0.16 ± 0.03 vs. 0.06 ± 0.01 for WD, $P = 0.01$; Fig. 4 *A and B*), consistent with the results of capacitance jumps normalized to basal capacitance (Fig. 2 *B, D, and E*). The time courses of the fast (several milliseconds) and slow (tens of milliseconds) components of transmitter release were similar at P8–14, P16–25, and P16–25 with WD (*SI Appendix, Fig. S7 A and B*). Because the fast component of transmitter release is thought to be responsible for the synchronized transmitter release induced by APs (28, 36), we examined the number of vesicles released in response to AP-like stimulation (1-ms depolarization to +40 mV). The AP-like stimulation evoked the release of more vesicles at P16–25 than at P8–14 or under the WD condition (Fig. 4 *C and D*). Furthermore, we calculated the release probability evoked by the AP-like stimulation (P_{TAP}) by comparing the AP-like stimulation-evoked release number against the fast component size or the total RRP size. P_{TAP} per the fast component at P16–25 was somewhat larger than at P8–14 and under the WD condition, but these had large amounts of variability caused by the small sizes of the fast component (*SI Appendix, Fig. S8A*). However, P_{TAP} per RRP was significantly larger at P16–25 than at P8–14 or under WD conditions (*SI Appendix, Fig. S8B*). Thus, a larger fraction of the RRP was triggered for exocytosis by an AP-like stimulation at

Whisker (Krox20(+))

Ectopic (Krox20(-))

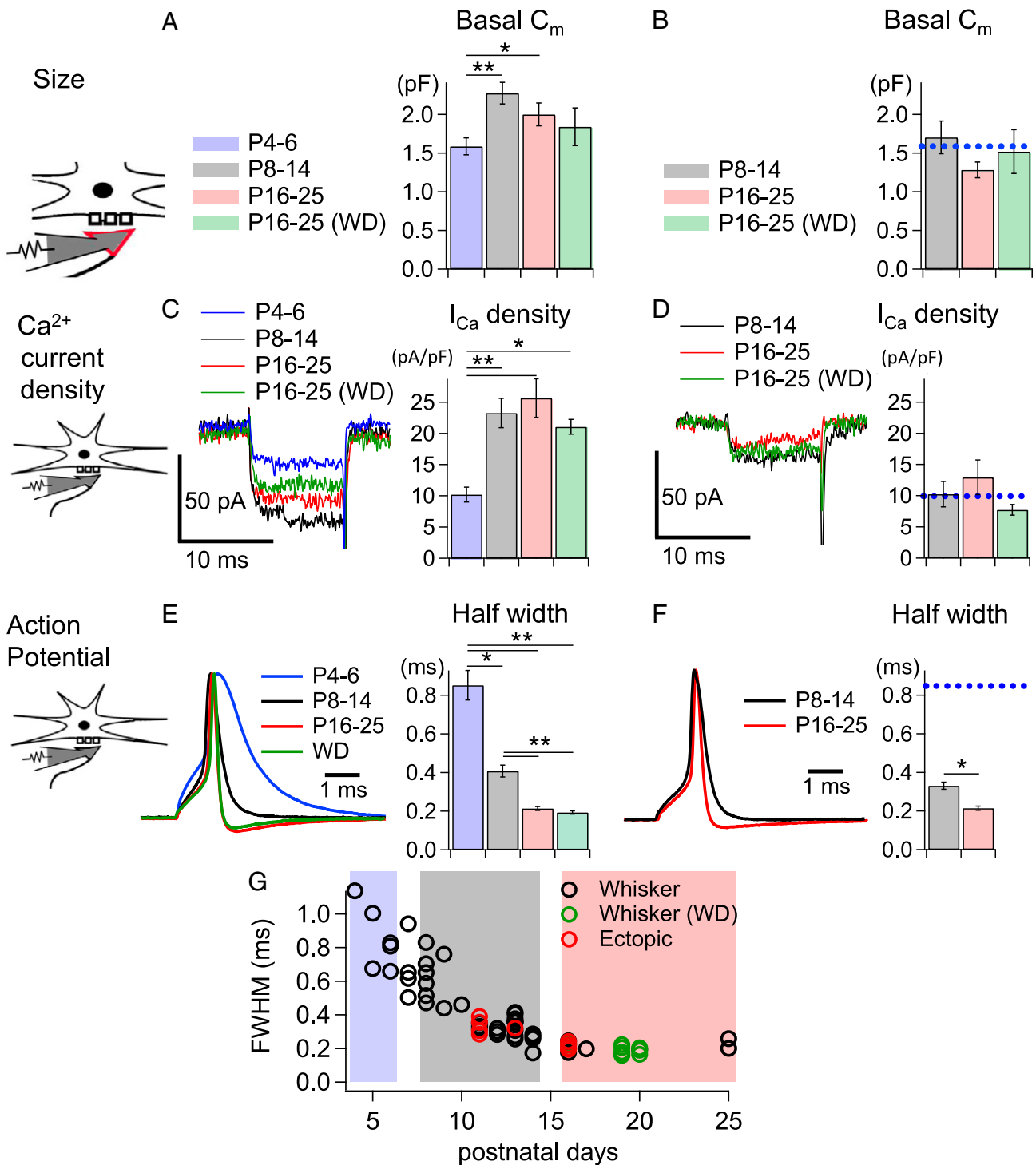


Fig. 3. Maturation of terminal sizes and calcium currents, but not action potential waveforms, are pathway specific. (A) Averaged basal capacitances under each condition at whisker-LFTs. $n = 21, 21, 37,$ and 31 for P4–6, P8–14, P16–25, and WD, respectively. (B) Same as in A but at ectopic-LFTs. $n = 11, 10,$ and 10.5 for P8–14, P16–25, and WD, respectively. (C) Example traces of calcium currents (Left) and averaged calcium current density (Right) induced by a 10-ms depolarization under each condition at whisker-LFTs. $n = 10, 34, 15,$ and 24 for P4–6, P8–14, P16–25, and WD, respectively. (D) Same as in C but at ectopic-LFTs. $n = 6, 5,$ and 5 for P8–14, P16–25, and WD, respectively. (E) Example of normalized APs (Left) and averaged AP half width (Right) under each condition at whisker-LFTs. $n = 6, 28, 8,$ and 10 for P4–6, P8–14, P16–25, and WD, respectively. (F) Same as in E but at ectopic-LFTs. $n = 5$ and 4 for P8–14 and P16–25, respectively. (G) The AP FWHM values were plotted against postnatal days. Blue dotted lines in B, D, and F show values of P4–6 whisker-LFTs for comparison. $*P < 0.05,$ $**P < 0.01,$ one-way ANOVA followed by Tukey's post hoc test. Error bars show SEMs. In the calcium currents shown in C and D, the capacitive artifact might have been emphasized by the leak subtraction procedure (see Methods).

P16–25 than at P8–14 or under WD conditions, most likely a result of the larger fast component. These results strongly suggest that the larger fast component is advantageous for AP-evoked transmitter release *in vivo*.

Fast Component of Transmitter Release Is Mediated by Vesicles Tightly Coupled to Calcium Channels. In general, transmitter release from the presynaptic terminal is triggered by calcium influx through voltage-gated calcium channels (VGCCs). Thus, the development of the fast component of transmitter release may reflect enhanced coupling of VGCCs to fast-releasing vesicles (18). The coupling distance between VGCCs and releasable vesicles can be examined by investigating the sensitivity to a calcium chelator, e.g., EGTA (ethylene glycol tetraacetic acid), as a large amount of intracellular EGTA predominantly blocks exocytosis of loosely coupled releasable vesicles (9, 37). Therefore, the spatial coupling properties of VGCCs and releasable vesicles can be examined by measuring the capacitance jump blockade induced by EGTA dialysis.

We increased the intracellular concentration of EGTA from 0.1 mM to 5 mM and examined the time course of transmitter release under each condition by capacitance measurements. The larger amount of EGTA strongly reduced maximum capacitance jumps of whisker-LFTs at P8–14, at P16–25, and under WD conditions (Fig. 5*A* and *B*), but the amount of blockade against shorter depolarizations was significantly smaller at P16–25 whisker-LFTs (Fig. 5*A–C*). The results indicate that the enlargement of the fast component of transmitter release was caused by tighter coupling of VGCCs to fast-releasing vesicles. This process occurred between P8–14 and P16–25 (i.e., between functional differentiation and mature phases) in an experience-dependent manner.

Discussion

In this study, we directly examine the transmitter release kinetics from presynaptic terminals fated for survival or for elimination during development in the mammalian central nervous system. The unique features of LFT-VPM neuron synapses provide 1)

direct accessibility of presynaptic terminals with the patch-clamp technique, 2) clear distinction of terminals that will survive and those to be eliminated during development, and 3) controllability of pathway-specific whisker sensory-mediated inputs for surviving presynaptic terminals. We show that transmitter release mechanisms develop at these so-called whisker-LFTs but not at ectopic-LFTs that are fated for elimination. Deprivation of sensory experience prevents the maturation of transmitter release machinery at whisker-LFTs but does not promote the development of the transmitter release machinery at ectopic-LFTs. In contrast to the transmitter release kinetics, the developmental shortening of AP waveforms is comparable between whisker- and ectopic-LFTs and shows no experience dependence. Taken together, we propose that sensory experience affects synapse development independently at whisker- and ectopic-LFTs of the somatosensory thalamus. At whisker-LFTs, sensory experience drives the development of specific elements of transmitter release machinery. By contrast, sensory experience does not affect functional differentiation at ectopic-LFTs but rather promotes structural pruning (7).

A Large Pool of Releasable Vesicles and Fast Component at Whisker-LFTs. Our results indicate the presence of a very large pool of releasable vesicles at whisker-LFTs. The RRP per pF (300 vesicles) of the mature whisker-LFTs is within the range of previously reported sizes at other large presynaptic terminals, such as calyx of Held terminals (35 to 400 vesicles/pF) (15, 38–40), mossy fiber boutons of hippocampus (1,000 vesicles/pF) (11), and mossy fiber boutons of the cerebellum (250 to 500 vesicles/pF) (12, 31). Given that our recordings are biased to large and isolated terminals and that the basal membrane capacitances (~2 pF) are similar to those of hippocampal mossy fiber boutons (41), our data represent LFTs of large size (~4- μ m diameter) (42, 43). The number of active zones within an average-sized LFT with a 2- μ m diameter is estimated to be three in mature mice (42). Thus, the number of active zones within a single LFT in our recordings is estimated to be ~10. The fraction

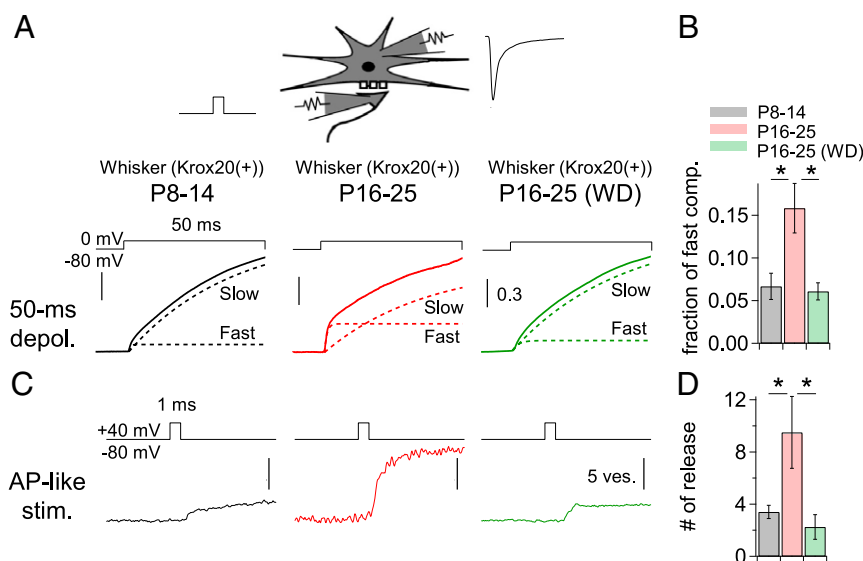


Fig. 4. Fast component of transmitter release is more efficiently triggered for release by AP-like stimulations at whisker-LFTs. (A) Example of cumulative release kinetics estimated from EPSC deconvolutions evoked by a 50-ms depolarization under each condition. Fast and slow components are shown superimposed as dotted lines. Schematic view of paired-recording configuration is shown on the Top. (B) Averaged fractions of the fast component under each condition. $n = 8, 8,$ and 7 for P8–14, P16–25, and WD, respectively. (C) Example release number estimated from EPSC deconvolutions evoked by an AP-like stimulus under each condition. (D) Averaged number of released vesicles under each condition. $n = 10, 8,$ and 7 for P8–14, P16–25, and WD, respectively. $*P < 0.05$, one-way ANOVA followed by Tukey's post hoc test. Error bars show SEMs.

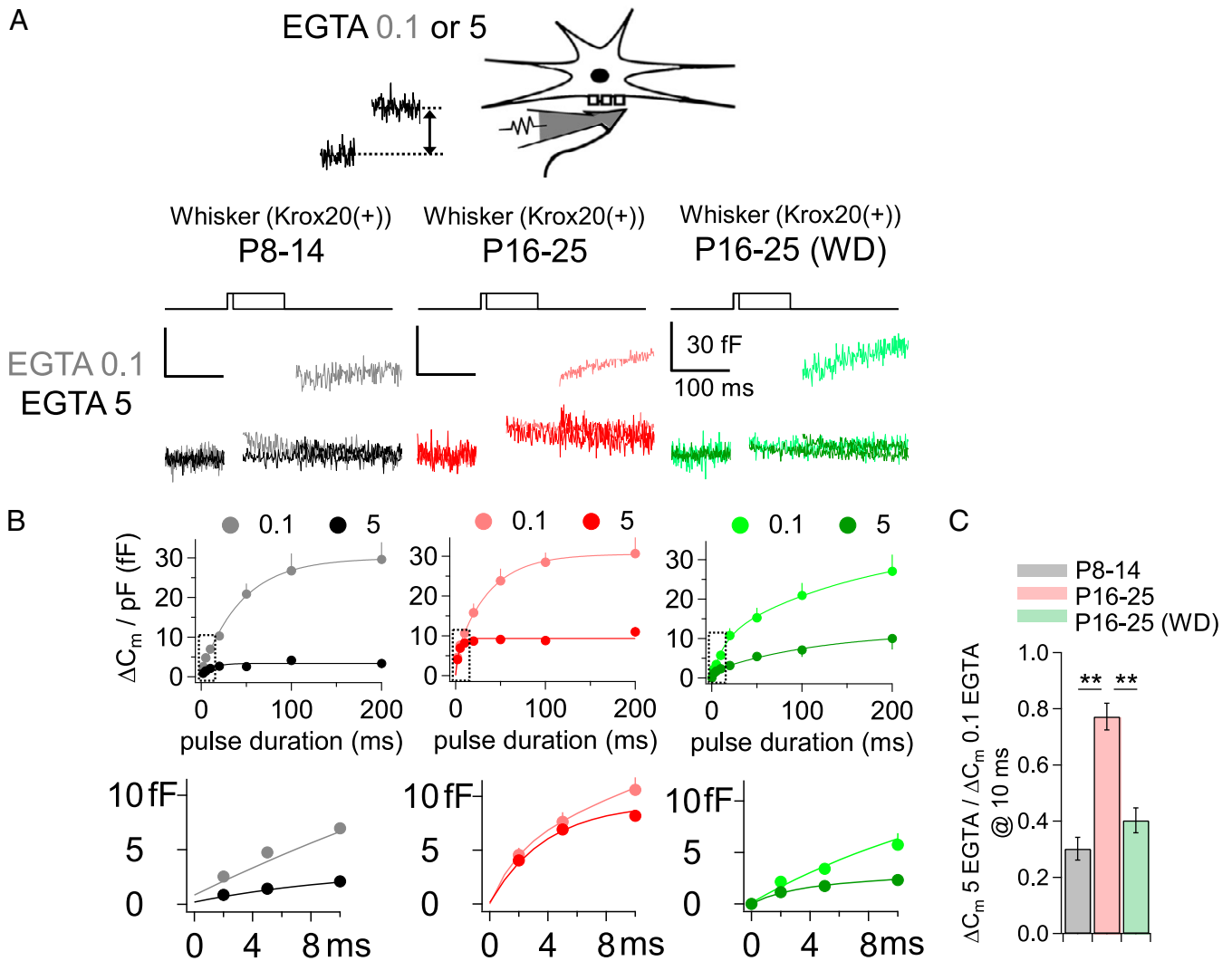


Fig. 5. Fast component of transmitter release is mediated by vesicles tightly coupled to VGCCs at whisker-LFTs. (A) Example of capacitance jumps induced by 10- and 100-ms depolarizations under each condition with 0.1 mM or 5 mM EGTA internal solutions. Schematic view of capacitance measurement configuration is shown on the *Top*. (B) Averaged ΔC_m per pF values were plotted against pulse durations under each condition with 0.1 mM or 5 mM EGTA internal solutions. *Bottom* shows enlarged traces of boxed regions. (C) Averaged fractions of ΔC_m evoked by a 10-ms depolarization in 5 mM EGTA compared with those in 0.1 mM EGTA. $n = 4, 18,$ and 12 for P8-14, P16-25, and WD, respectively. $**P < 0.01$, one-way ANOVA followed by Tukey's post hoc test. Error bars show SEMs.

of the fast component of transmitter release calculated from EPSC deconvolution was ~ 0.15 (Fig. 4), which corresponds to 4.5 fF/pF assuming a total RRP size of 30 fF/pF (Fig. 2). Again, by scaling this value for a basal membrane capacitance of 2 pF, the size of the fast component is ~ 9 fF, or ~ 90 vesicles per terminal. Thus, each active zone contains ~ 9 fast-releasing vesicles. The number is higher than reported for large presynaptic terminals (11, 13) but matches well with the number of docked vesicles within a single active zone at a small conventional-sized excitatory glutamatergic synapse (44, 45).

The total RRP size of mature whisker-LFTs was 60 fF (30 fF/pF \times 2 pF), or ~ 600 vesicles, which translates to ~ 60 vesicles per active zone. The number is much higher than that for other depressive large presynaptic terminals, such as the calyx of Held (3 to 6) (46) or cerebellar mossy fiber boutons (3) (12), and is even higher than that for facilitative hippocampal mossy fiber boutons (30) (11). The large RRP and depressive property of the LFTs suggests a slow but massive amount of replenishment. We note that the total RRP size estimated from the capacitance

jump evoked by a long depolarization in this study may include replenished vesicles during the stimulus; thus the number could be an overestimation.

Developmental Maturation of Release Machinery at Whisker-LFTs.

Synapses change their morphological and functional properties during their development from immature to mature states, and newly formed immature synapses often possess functional properties distinct from those of mature synapses (47). Unlike postsynaptic developmental maturation that has been relatively well documented, the small sizes of presynaptic terminals at most synapses in the central nervous system have prevented direct measurements of their developmental maturation. The giant terminal of the calyx of Held synapse is an exception, and the developmental changes of their presynaptic properties have been explored extensively (14–20). Those studies indicated that the calyx of Held terminal becomes functionally mature just before the onset of hearing (\sim P14 in rodents); thus the transmitter release mechanisms mature independently of sound experience

(48). Studies of lemniscal fiber-VPM neuron synapses have indicated that the synaptic wiring matures at around P16 (4, 7), and our study found that the release machinery of whisker-LFTs matures at around the same age. However, the whisker sensory pathway is already active well before this timepoint, as a passive whisker deflection is thought to be crucial for suckling at a few days after birth (49), and active whisking begins at P14 (50). The different timings of synaptic maturation compared with sensory onset are of interest. Because the enlargement of the fast component of transmitter release occurs just after active whisking begins, and WD prevents this enlargement, active whisking may be crucial for functional maturation. Despite our finding that the maturation of the presynaptic release properties and synaptic wiring are highly correlated, causation cannot currently be established and remains to be elucidated.

It is interesting to note that the development of the transmitter release mechanism is pathway and experience dependent, whereas developmental shortening of AP waveforms is pathway and experience independent. The results suggest that the construction of release units by active zone scaffolds (e.g., neurexins, RIMs, and Munc13) (51, 52), but not AP waveform regulating ion channels (e.g., N^+ and K^+ channels) (35, 53), is pathway and experience dependent, and that VGCCs are recruited to these release units for tight couplings between VGCCs and release sites (54, 55). Alternatively, it is also possible that the extreme changes in the calcium sensitivity of the vesicles for exocytosis may underlie the enlargement of the fast component of the RRP.

Developmental Changes of Release Machinery at Ectopic-LFTs. The elimination of early-formed unnecessary synapses is crucial for the formation of mature functional neural circuits. However, presynaptic properties of the to-be-pruned terminals remain unknown, as recordings from presynaptic terminals that are known to be eliminated after maturation were impossible. In this study, we selectively recorded presynaptic terminals fated for elimination by taking advantage of genetic and viral labeling. Our data clearly indicate that the RRP of these terminals remain small and never enlarge (Fig. 2). The calcium currents and the basal membrane capacitances (i.e., terminal sizes) also remain small, which suggests that the release properties of ectopic-LFTs remain immature throughout development. Given that WD (i.e., inhibition of whisker-LFTs) does not promote the strengthening of ectopic-LFTs, it is suggested that sensory experience-dependent functional developments of “winner” fibers and “loser” fibers do not interfere with each other. On the other hand, the elimination of loser fiber synapses is prevented by WD (7), indicating that the structural pruning is an experience-dependent process.

In contrast to the RRP size, the AP waveform at ectopic-LFTs becomes shorter with development similarly to whisker-LFTs. The shorter presynaptic APs are usually associated with smaller EPSCs because of the decreased release probability as a result of shorter calcium influx (18, 56). Therefore, our results suggest that the synaptic transmission from ectopic-LFTs in vivo becomes gradually unreliable with development as a result of the progressive shortening of APs without RRP enlargement, unlike at whisker-LFTs, where RRP enlargement balances the decrease of release probability caused by AP shortenings, as reported at calyx of Held synapses (57). Given the previous findings that a VPM neuron is innervated by a single whisker fiber after P16 (7), AP-evoked transmitter release from ectopic-LFTs is not capable of evoking a postsynaptic response and/or the corresponding postsynaptic structure is lost.

At the climbing fiber-to-Purkinje cell synapse, the sizes of postsynaptic densities formed by weak (putative “loser”) fibers are indistinguishable from those formed by strong (putative “winner”) fibers in the functional differentiation phase (58). On the other hand, at the immature calyx of Held synapse, the synaptic contact area of the large (putative winner) terminals is

clearly larger than that of the small (putative loser) terminals (59). Our results indicate that at LFT-VPM neuron synapses, transmitter release kinetics are clearly distinguishable between whisker- and ectopic-LFTs in the functional differentiation phase, and WD does not affect the transmitter release from ectopic-LFTs (Fig. 2). This is consistent with our previous morphological finding that ectopic-LFTs are smaller than whisker-LFTs, and WD did not promote enlargement of the ectopic-LFTs (7). It will be interesting to examine the morphological difference between whisker- and ectopic-LFTs in more detail (e.g., distribution of synaptic vesicles) in the future.

It should be noted that technical limitations biased our recordings to large terminals; thus small terminals were essentially ignored in this study. We normalized the responses to the basal capacitance to mitigate this, but we cannot rule out the possibility that small responses of ectopic-LFTs, nevertheless, might be overestimated, and that the difference between whisker- and ectopic-LFTs may be even larger. We should also mention the lack of Krox20 at ectopic-LFTs. Because Krox20 is a transcription factor with many targets, many parameters other than pool maturation could be different between Krox20(+) whisker-LFTs and Krox20(−) ectopic-LFTs.

Comparison with Remodeling of Other Neuronal Circuits. Developmental synapse refinement has been extensively studied in several regions in the brain (3–6), particularly, cerebellar climbing fiber-to-Purkinje cell synapses and retinogeniculate synapses in the lateral geniculate nucleus. In these areas, the presynaptic functional differences between strong and weak fibers (60, 61), or undeveloped and developed fibers (33), have been proposed based on recordings of postsynaptic responses. The studies suggest that at strong or developed presynaptic terminals, the number of released vesicles/AP is increased, and the AP-induced transmitter release is more synchronized. Our results directly demonstrate that the development of the fast component of transmitter release is the underlying mechanism.

In the lateral geniculate nucleus, changes to the terminal (or bouton) clustering (but not axon retraction) contribute to synapse refinement during the functional differentiation phase. We previously showed that a proportion of ectopic-LFTs (~13% of the total) structurally remain in the VPM after single-fiber innervation is established (i.e., after synaptic connections mediated by ectopic-LFTs are eliminated) (7). In this study, we confirmed this finding, with ectopic-LFTs remaining at P16–25, indicating that fibers with inputs that are fated for elimination remain in the VPM. Together with our previous finding that the number of input fibers can increase after circuit maturation via peripheral afferent nerve cutting (7), it is likely that synapse elimination precedes axon retraction in the VPM as well as in the lateral geniculate nucleus. It is interesting to note that the number of presynaptic terminals formed by the afferent fiber with the strongest input in a mature circuit (~60) is similar between retinogeniculate synapses and LFT-VPM neuron synapses (62, 63). It is not clear whether similar changes to terminal (or bouton) clustering occur and contribute to climbing fiber-to-Purkinje cell synapse refinement in the developing cerebellum.

To gain a general view of neuronal circuit formation, it is crucial to investigate the similarities and differences between the different models of developmental synapse refinement. Our findings shed light on this and on the synapse elimination theory, which may help to reveal a common principle of neuronal circuit formation.

Methods

Experimental Animals. All experiments were approved by the animal care and use committee of the Tokyo Women’s Medical University, and were performed according to the institutional guidelines concerning the care and handling of experimental animals. Krox20-Cre mice (JAX#025744) (21) were backcrossed to C57BL/6 mice for more than three generations before use.

Cre-dependent synaptophysin-tdTomato reporter mice (Ai34D) [B6;129SvEv-Tg(ROSA)26Sortm34.1(CAG-SyptdTomato)Hze/J; JAX#012570] (22) were obtained from The Jackson Laboratory. To visualize PrV2-originating lemniscal fibers, male Krox20-Cre heterozygotes and female Ai34D homozygotes or heterozygotes were crossed, and Cre⁺ pups (Krox20-Ai34D mice) were used. Krox20-Ai34D pups were detected by tdTomato signals in vibrissal follicles expressed beginning at late pregnancy. Male and female mice (P4 to P25) were used. All efforts were taken to minimize animal numbers.

Preparation of Acute Thalamic Slices. Mice were deeply anesthetized with isoflurane (Abbott) and decapitated, and brains were removed in accordance with the guidelines of the Physiological Society of Japan. Parasagittal thalamic slices 200 to 300 μ m thick were obtained using a Leica VT1200S microslicer (Leica Microsystems) in ice-cold slice medium containing the following (in millimoles): 234 sucrose, 2.5 KCl, 1.25 NaH₂PO₄, 10 MgCl₂, 0.5 CaCl₂, 25 NaHCO₃, 0.5 myo-inositol, and 11 glucose equilibrated with 95% O₂ and 5% CO₂. Slices were then incubated at 32 °C for >0.5 h in an artificial cerebrospinal fluid (ACSF) containing the following (in millimoles): 125 NaCl, 2.5 KCl, 1.25 NaH₂PO₄, 1 MgCl₂, 2 CaCl₂, 26 NaHCO₃, 20 glucose (pH 7.4, gassed with 95% O₂ and 5% CO₂). Slices were visualized with IR-DIC (infrared-differential interference contrast) on an upright microscope (BX-51, Olympus) in a recording chamber filled with ACSF. A slice in a recording chamber was perfused with 30 to 32 °C ACSF at a rate of 2.5 to 3.0 mL/min. PrV2-originating LFTs of Krox20-Ai34D mice were identified by 565 nm LED (light emitting diode) (Thorlabs) excitation. Non-PrV2-originating LFTs of AAV9-Ef1a-DO-ChETA-EYFP-WPRE-pA-injected Krox20-Ai34D mice were identified by 470 nm LED (Thorlabs) excitation. Both IR-DIC and the fluorescence of tdTomato or EYFP were imaged with an sCMOS camera (Zyla; Andor), controlled by SOLIS software (Andor). During terminal recordings with capacitance measurements, 1 μ M tetrodotoxin (TTX) and 10 mM tetraethylammonium chloride (TEA-Cl) were added to block Na⁺ and K⁺ channels. For paired recordings, 50 μ M AP5 and 100 μ M cyclothiazide were included to block NMDA (N-methyl-D-aspartate) receptors and the desensitization of AMPA receptors, respectively. For terminal recordings with AP measurements, all blockers were removed. Recordings were performed within 6 h after cutting the slices. For EPSC recordings with external stimulation, 10 μ M (-)-bicuculline methochloride, 50 μ M AP5, and 100 μ M cyclothiazide were added to block GABA [γ (gamma)-aminobutyric acid] receptors, NMDA receptors, and the desensitization of AMPA receptors, respectively.

Whole-Cell Recordings. LFTs were whole-cell voltage clamped at -70 mV using an EPC10/2 amplifier (HEKA) controlled by PatchMaster software (HEKA). The patch pipettes were filled with intracellular solution containing the following (in millimoles): 135 Cs-gluconate, 20 TEA-Cl, 10 Hepes, 5 Na₂-phosphocreatine, 4 Mg adenosine triphosphate (MgATP), 0.3 Na guanosine triphosphate (NaGTP), 5 QX-314, and 0.1 EGTA (pH 7.2). In some experiments, EGTA was raised to 5 mM. Membrane currents were low-pass filtered at 3 kHz and sampled at 20 to 100 kHz. Leak currents were subtracted using appropriately scaled responses against small voltage steps (usually 20% of the test step) to measure the calcium currents. Data were analyzed off-line with IgorPro software (Wavemetrics). Membrane capacitance measurements were performed using an EPC10/2 amplifier in the sine + DC configuration. A sine wave (30 mV in amplitude, 1,000 Hz in frequency) was superimposed on a holding potential of -80 mV. To evoke exocytosis, depolarizing pulses to 0 mV were applied. To limit the membrane capacitance (C_m) change to a single presynaptic terminal, recordings were made from isolated terminals with few neighboring varicosities. Patch pipettes (Harvard, GC150F-10) typically had a resistance of ~12 M Ω , and the average series resistance was ~50 M Ω , which was similar to previously reported values for small presynaptic recordings (41). We stopped recordings when the leak currents exceeded 100 pA at resting potential. Depolarizing pulses were applied every minute to allow for complete recovery of responses from depression. For AP recordings, Cs-gluconate and TEA-Cl were replaced by K-gluconate, and QX-314 was omitted. APs were induced by 1-ms current injections.

VPM neurons were whole-cell clamped at -70 mV with a patch pipette (Harvard, GC150-10) with a resistance of ~4 M Ω . Average series resistance was <15 M Ω , which was compensated so that residual resistance was ~3 M Ω . For VPM neuron recordings, TEA-Cl was removed, and EGTA was raised to 1 mM in the intracellular solution. To evoke lemniscal fiber-mediated EPSCs, a concentric bipolar electrode (tip diameter, 25 μ m) (IMB-16820; Inter-Medical) was used. The stimulus electrode was placed on the medial lemniscal fiber bundle (4, 7), and a 100 μ s electrical square pulse was applied. We ensured that recorded EPSCs were from lemniscal fibers, not from corticothalamic fibers, according to established criteria (7): depression of EPSCs in

response to paired-pulse stimuli and all-or-none responses with distinct thresholds in response to increasing stimulus intensity. Lemniscal fiber-mediated EPSCs displayed the paired-pulse depression throughout development in the absence of cyclothiazide (4).

Whisker Deprivation. All unilateral mystacial vibrissae on the snout were deprived every other day from P12–13 to the slice recording day, ranging from P16 to P25. Under a dissecting microscope, vibrissae of isoflurane-anesthetized mice were carefully plucked out using fine tweezers by applying slow and steady tension to the base of the vibrissa until the vibrissa slipped out of the follicle (24).

Viral Vector Construction and Stereotaxic Surgery. To express fluorescent proteins selectively in Cre⁻ non-PrV2-originating lemniscal fibers, we used the viral vector AAV9-Ef1a-DO-ChETA-EYFP-WPRE-pA (23). AAV9 viral particles were kindly packaged and purified by the Gunma University Initiative for Advanced Research Viral Vector Core. The genomic titer of the purified AAV9 viral particles as determined by real-time PCR was 1.65×10^{13} vector genomes/mL. A standard stereotaxic injection surgery (24) was made under isoflurane (3% for induction, 2% for maintenance) anesthesia and local lidocaine (2%) analgesia. In brief, the head of a P3 to P7 mouse pup was fixed on a stereotaxic apparatus, and a dorsal midline skin incision was made to align the bregma and lambda points. A small hole was made in the skull above the left occipital cortex with a HP1/4 carbide bar (Midwest) attached to a hand grinder (V112J; Minitor), and 1 μ L AAV9 vector was injected into the left Pr5 (4.2 to 4.3 mm posterior and 1.7 to 1.8 mm lateral from the bregma, 3.7 to 3.8 mm below the dura) through a microneedle syringe (NF35BV and NANOFIL; WPI) by continuous pressure from a microsyringe pump (Micro4; WPI). After injection, the needle tip was held in the Pr5 for 5 min. After the injection, the wound was stitched with nylon sutures, and mice were returned to their mothers for recovery. Slice experiments were conducted 5 to 18 d after injection. Because it was necessary to wait more than 5 d for sufficient expression of the fluorescent protein (EYFP), the recordings from the ectopic-LFTs were performed only after P8.

Immunohistochemistry. Brainstem regions of the AAV9-Ef1a-DO-ChETA-EYFP-WPRE-pA-injected Krox20-Ai34D mice used to prepare the thalamic slices were fixed with 4% paraformaldehyde and 0.2% picric acid in 0.1 M phosphate-buffered solution (PBS) at least overnight and then coronally cut into 100- μ m sections using a vibratome (Leica VT1000; Leica Microsystems). Sections were incubated overnight at 4 °C with a rat monoclonal antibody against GFP (Nacalai Tesque; 1:1,000) and a rabbit polyclonal antibody against RFP (Rockland; 1:1,000) in 0.05 M PBS containing 10% normal donkey serum and 0.3% Triton X-100. After washing in PBS, the sections were reacted with secondary antibodies conjugated to Alexa Fluor 488 (for GFP) (Abcam; 1:500) and Alexa Fluor 647 (for RFP) (Abcam; 1:500) for 2 h at room temperature or overnight at 4 °C. To quantify EYFP and tdTomato expression using an epifluorescence upright microscope (BX-51; Olympus), sections were mounted on glass slides, sealed with SlowFade Diamond antifade mountant (Thermo Fisher Scientific), and coverslipped with spacers (50 μ m depth \times 3). Images were acquired using a 5 \times lens objective and a sCMOS camera (Zyla; Andor), controlled by SOLIS software (Andor).

Analysis. Data were analyzed using IgorPro and Excel (Microsoft). Transmitter release rates were calculated by deconvolving EPSCs with the mEPSCs (26, 27). The mEPSC amplitudes were measured by detecting asynchronous release events following the stimulation. The EPSCs were assumed to be a linear summation of mEPSCs and have no residual currents due to delayed clearance of glutamate in the synaptic cleft (27). The calculated release rates were validated by comparing the cumulative release with capacitance jumps.

Quantification and Statistical Analysis. Means and SEs were calculated in Igor or Excel. Data are presented as means \pm SEMs. *P* values were determined with two-tailed Student's *t* test or ANOVA. Details, including sample sizes, can be found in figure legends.

Data Availability. All study data are included in the article and/or supporting information.

ACKNOWLEDGMENTS. We thank Hisako Nakayama for critical reading of the manuscript and helpful comments; Yumi Tani and Sachie Sekino for technical support; Takuji Iwasato for kindly providing Krox20-Cre mice; and

the Gunma University Initiative for Advanced Research Viral Vector Core for kindly packaging and purifying AAV9 viral particles. This work was supported by the Japan Society for the Promotion of Science (JSPS) Grants-in-Aid for Scientific Research (KAKENHI) Grants (17K19466 and 17H03548 to M. Midorikawa and 19H03343, 17H05752, and 16H01344 to M. Miyata); Grant-in-Aid for Transformative Research Areas (Grant 20H05916 to M. Miyata); the

Takeda Science Foundation (to M. Midorikawa), the SHISEIKAI Scholarship Fund for Basic Researcher of Medical Science, Keiko Watanabe Award (to M. Miyata); and the program for Brain Mapping by Integrated Neurotechnologies for Disease Studies (Brain/MINDS) from the Japan Agency for Medical Research and Development (under Grant JP19dm0207057 to the Gunma University Initiative for Advanced Research Viral Vector Core).

1. L. C. Katz, C. J. Shatz, Synaptic activity and the construction of cortical circuits. *Science* **274**, 1133–1138 (1996).
2. A. Holtmaat, K. Svoboda, Experience-dependent structural synaptic plasticity in the mammalian brain. *Nat. Rev. Neurosci.* **10**, 647–658 (2009).
3. J. W. Lichtman, H. Colman, Synapse elimination and indelible memory. *Neuron* **25**, 269–278 (2000).
4. D. Arsenault, Z. W. Zhang, Developmental remodelling of the lemniscal synapse in the ventral basal thalamus of the mouse. *J. Physiol.* **573**, 121–132 (2006).
5. B. M. Hooks, C. Chen, Circuitry underlying experience-dependent plasticity in the mouse visual system. *Neuron* **106**, 21–36 (2020).
6. M. Kano, T. Watanabe, N. Uesaka, M. Watanabe, Multiple phases of climbing fiber synapse elimination in the developing cerebellum. *Cerebellum* **17**, 722–734 (2018).
7. Y. Takeuchi *et al.*, Large-scale somatotopic refinement via functional synapse elimination in the sensory thalamus of developing mice. *J. Neurosci.* **34**, 1258–1270 (2014).
8. H. von Gersdorff, G. Matthews, Dynamics of synaptic vesicle fusion and membrane retrieval in synaptic terminals. *Nature* **367**, 735–739 (1994).
9. J. G. Borst, B. Sakmann, Calcium influx and transmitter release in a fast CNS synapse. *Nature* **383**, 431–434 (1996).
10. J. G. Borst, F. Helmchen, B. Sakmann, Pre- and postsynaptic whole-cell recordings in the medial nucleus of the trapezoid body of the rat. *J. Physiol.* **489**, 825–840 (1995).
11. S. Hallermann, C. Pawlu, P. Jonas, M. Heckmann, A large pool of releasable vesicles in a cortical glutamatergic synapse. *Proc. Natl. Acad. Sci. U.S.A.* **100**, 8975–8980 (2003).
12. A. Ritzau-Jost *et al.*, Ultrafast action potentials mediate kilohertz signaling at a central synapse. *Neuron* **84**, 152–163 (2014).
13. N. P. Vyleta, P. Jonas, Loose coupling between Ca²⁺ channels and release sensors at a plastic hippocampal synapse. *Science* **343**, 665–670 (2014).
14. H. Taschenberger, H. von Gersdorff, Fine-tuning an auditory synapse for speed and fidelity: Developmental changes in presynaptic waveform, EPSC kinetics, and synaptic plasticity. *J. Neurosci.* **20**, 9162–9173 (2000).
15. H. Taschenberger, R. M. Leão, K. C. Rowland, G. A. Spirou, H. von Gersdorff, Optimizing synaptic architecture and efficiency for high-frequency transmission. *Neuron* **36**, 1127–1143 (2002).
16. M. J. Fedchyshyn, L. Y. Wang, Developmental transformation of the release modality at the calyx of Held synapse. *J. Neurosci.* **25**, 4131–4140 (2005).
17. A. Rodríguez-Contreras, J. S. van Hoeve, R. L. Habets, H. Locher, J. G. Borst, Dynamic development of the calyx of Held synapse. *Proc. Natl. Acad. Sci. U.S.A.* **105**, 5603–5608 (2008).
18. Y. Nakamura *et al.*, Nanoscale distribution of presynaptic Ca²⁺ channels and its impact on vesicular release during development. *Neuron* **85**, 145–158 (2015).
19. O. Kochubey, N. Babai, R. Schneggenburger, A synaptotagmin isoform switch during the development of an identified CNS synapse. *Neuron* **90**, 984–999 (2016).
20. C. I. Thomas *et al.*, Presynaptic mitochondria volume and abundance increase during development of a high-fidelity synapse. *J. Neurosci.* **39**, 7994–8012 (2019).
21. O. Voiculescu, P. Charnay, S. Schneider-Maunoury, Expression pattern of a Krox-20/Cre knock-in allele in the developing hindbrain, bones, and peripheral nervous system. *Genesis* **26**, 123–126 (2000).
22. L. Madisen *et al.*, A robust and high-throughput Cre reporting and characterization system for the whole mouse brain. *Nat. Neurosci.* **13**, 133–140 (2010).
23. A. Saunders, C. A. Johnson, B. L. Sabatini, Novel recombinant adeno-associated viruses for Cre activated and inactivated transgene expression in neurons. *Front. Neural Circuits* **6**, 47 (2012).
24. Y. Takeuchi, H. Osaki, Y. Yagasaki, Y. Katayama, M. Miyata, Afferent fiber remodeling in the somatosensory thalamus of mice as a neural basis of somatotopic reorganization in the brain and ectopic mechanical hypersensitivity after peripheral sensory nerve injury. *eNeuro* **4**, ENEURO.0345-16.2017 (2017).
25. E. Neher, A. Marty, Discrete changes of cell membrane capacitance observed under conditions of enhanced secretion in bovine adrenal chromaffin cells. *Proc. Natl. Acad. Sci. U.S.A.* **79**, 6712–6716 (1982).
26. J. S. Diamond, C. E. Jahr, Asynchronous release of synaptic vesicles determines the time course of the AMPA receptor-mediated EPSC. *Neuron* **15**, 1097–1107 (1995).
27. E. Neher, T. Sakaba, Combining deconvolution and noise analysis for the estimation of transmitter release rates at the calyx of held. *J. Neurosci.* **21**, 444–461 (2001).
28. T. Sakaba, Roles of the fast-releasing and the slowly releasing vesicles in synaptic transmission at the calyx of Held. *J. Neurosci.* **26**, 5863–5871 (2006).
29. T. Yamashita, T. Hige, T. Takahashi, Vesicle endocytosis requires dynamin-dependent GTP hydrolysis at a fast CNS synapse. *Science* **307**, 124–127 (2005).
30. H. Wang, Z. W. Zhang, A critical window for experience-dependent plasticity at whisker sensory relay synapse in the thalamus. *J. Neurosci.* **28**, 13621–13628 (2008).
31. I. Delvendahl, S. Hallermann, The cerebellar mossy fiber synapse as a model for high-frequency transmission in the mammalian CNS. *Trends Neurosci.* **39**, 722–737 (2016).
32. T. Sakaba, E. Neher, Calmodulin mediates rapid recruitment of fast-releasing synaptic vesicles at a calyx-type synapse. *Neuron* **32**, 1119–1131 (2001).
33. J. L. Hauser, X. Liu, E. Y. Litvina, C. Chen, Prolonged synaptic currents increase relay neuron firing at the developing retinogeniculate synapse. *J. Neurophysiol.* **112**, 1714–1728 (2014).
34. N. Holderith *et al.*, Release probability of hippocampal glutamatergic terminals scales with the size of the active zone. *Nat. Neurosci.* **15**, 988–997 (2012).
35. Y. Nakamura, T. Takahashi, Developmental changes in potassium currents at the rat calyx of Held presynaptic terminal. *J. Physiol.* **581**, 1101–1112 (2007).
36. P. S. Kaeser, W. G. Regehr, The readily releasable pool of synaptic vesicles. *Curr. Opin. Neurobiol.* **43**, 63–70 (2017).
37. E. M. Adler, G. J. Augustine, S. N. Duffy, M. P. Charlton, Alien intracellular calcium chelators attenuate neurotransmitter release at the squid giant synapse. *J. Neurosci.* **11**, 1496–1507 (1991).
38. R. Schneggenburger, A. C. Meyer, E. Neher, Released fraction and total size of a pool of immediately available transmitter quanta at a calyx synapse. *Neuron* **23**, 399–409 (1999).
39. J. H. Bollmann, B. Sakmann, J. G. Borst, Calcium sensitivity of glutamate release in a calyx-type terminal. *Science* **289**, 953–957 (2000).
40. J. Y. Sun, L. G. Wu, Fast kinetics of exocytosis revealed by simultaneous measurements of presynaptic capacitance and postsynaptic currents at a central synapse. *Neuron* **30**, 171–182 (2001).
41. M. Midorikawa, T. Sakaba, Kinetics of releasable synaptic vesicles and their plastic changes at hippocampal mossy fiber synapses. *Neuron* **96**, 1033–1040.e3 (2017).
42. A. Graziano, X. B. Liu, K. D. Murray, E. G. Jones, Vesicular glutamate transporters define two sets of glutamatergic afferents to the somatosensory thalamus and two thalamocortical projections in the mouse. *J. Comp. Neurol.* **507**, 1258–1276 (2008).
43. C. Mo, I. Petrof, A. N. Víaene, S. M. Sherman, Synaptic properties of the lemniscal and paralemniscal pathways to the mouse somatosensory thalamus. *Proc. Natl. Acad. Sci. U.S.A.* **114**, E6212–E6221 (2017).
44. T. Schikorski, C. F. Stevens, Morphological correlates of functionally defined synaptic vesicle populations. *Nat. Neurosci.* **4**, 391–395 (2001).
45. M. A. Xu-Friedman, K. M. Harris, W. G. Regehr, Three-dimensional comparison of ultrastructural characteristics at depressing and facilitating synapses onto cerebellar Purkinje cells. *J. Neurosci.* **21**, 6666–6672 (2001).
46. E. Neher, T. Sakaba, Multiple roles of calcium ions in the regulation of neurotransmitter release. *Neuron* **59**, 861–872 (2008).
47. J. R. Sanes, J. W. Lichtman, Induction, assembly, maturation and maintenance of a postsynaptic apparatus. *Nat. Rev. Neurosci.* **2**, 791–805 (2001).
48. S. Oleskevich, M. Yousoufian, B. Walmsley, Presynaptic plasticity at two giant auditory synapses in normal and deaf mice. *J. Physiol.* **560**, 709–719 (2004).
49. H. Arakawa, R. S. Erzurumlu, Role of whiskers in sensorimotor development of C57BL/6 mice. *Behav. Brain Res.* **287**, 146–155 (2015).
50. R. S. Erzurumlu, P. Gaspar, Development and critical period plasticity of the barrel cortex. *Eur. J. Neurosci.* **35**, 1540–1553 (2012).
51. M. A. Böhme *et al.*, Rapid active zone remodeling consolidates presynaptic potentiation. *Nat. Commun.* **10**, 1085 (2019).
52. F. Luo, A. Sclip, M. Jiang, T. C. Südhof, Neurexins cluster Ca²⁺ channels within the presynaptic active zone. *EMBO J.* **39**, e103208 (2020).
53. M. H. Kole, J. J. Letzkus, G. J. Stuart, Axon initial segment Kv₁ channels control axonal action potential waveform and synaptic efficacy. *Neuron* **55**, 633–647 (2007).
54. R. G. Held *et al.*, Synapse and active zone assembly in the absence of presynaptic Ca²⁺ channels and Ca²⁺ entry. *Neuron* **107**, 667–683.e9 (2020).
55. M. Lübbert *et al.*, Cav_{v2.1} α1 subunit expression regulates presynaptic Cav_{v2.1} abundance and synaptic strength at a central synapse. *Neuron* **101**, 260–273.e6 (2019).
56. L. Y. Wang, L. K. Kaczmarek, High-frequency firing helps replenish the readily releasable pool of synaptic vesicles. *Nature* **394**, 384–388 (1998).
57. S. Iwasaki, T. Takahashi, Developmental regulation of transmitter release at the calyx of Held in rat auditory brainstem. *J. Physiol.* **534**, 861–871 (2001).
58. A. M. Wilson *et al.*, Developmental rewiring between cerebellar climbing fibers and purkinje cells begins with positive feedback synapse addition. *Cell Rep.* **29**, 2849–2861.e6 (2019).
59. M. C. Sierksma, J. A. Slotman, A. B. Houtsmuller, J. G. G. Borst, Structure-function relation of the developing calyx of Held synapse in vivo. *J. Physiol.* **598**, 4603–4619 (2020).
60. K. Hashimoto, M. Kano, Functional differentiation of multiple climbing fiber inputs during synapse elimination in the developing cerebellum. *Neuron* **38**, 785–796 (2003).
61. Y. Kawamura *et al.*, Spike timing-dependent selective strengthening of single climbing fibre inputs to Purkinje cells during cerebellar development. *Nat. Commun.* **4**, 2732 (2013).
62. P. Veinante, M. Deschênes, Single- and multi-whisker channels in the ascending projections from the principal trigeminal nucleus in the rat. *J. Neurosci.* **19**, 5085–5095 (1999).
63. J. L. Morgan, D. R. Berger, A. W. Wetzel, J. W. Lichtman, The fuzzy logic of network connectivity in mouse visual thalamus. *Cell* **165**, 192–206 (2016).